CHARACTERIZATION OF COLD MODEL CAVITY OF CRYOCOOLED C-BAND 2.6-CELL RF GUN AT 20 K *

T. Tanaka[†], T. Sakai, K. Nogami, K. Hayakawa, Y. Hayakawa, K. Nakao, K. Takatsuka, LEBRA, Nihon University, Funabashi, Japan

M. Fukuda, D. Satoh, T. Takatomi, N. Terunuma, J. Urakawa, M. Yoshida, KEK, Tsukuba, Japan

Abstract

A cryogenic C-band 2.6-cell photocathode RF electron gun has been studied at Nihon University in collaboration with KEK for future use in a compact electron-accelerator based monochromatic X-ray source. The cold model cavity with an input coupler was fabricated at KEK in 2016 by ultraprecision machining and diffusion bonding techniques. The RF characteristics of the cavity obtained at cryogenic measurements have been in agreement with the result of the CST Studio simulation. The unloaded quality factor of ~73000 has been obtained at the cavity temperature of 20 K, which is 5.5 times higher than that at room temperature and consistent with the simulation taking into account the anomalous skin effect of the cavity surface resistance. The input coupling coefficient of approximately 20 at 20 K has well reproduced the design value. The shift in the accelerating π-mode resonant frequency due to the cavity temperature change from 296.65 to 20 K has been 19.02 MHz, being 0.12 MHz greater than the value based on the linear expansion coefficients for copper by NIST.

INTRODUCTION

An RF cavity made of high-purity copper operating at low temperatures is known to be low power loss due to low surface resistance compared to room temperature operation [1, 2], though the effect is not as drastic as a superconducting cavity. In addition, significantly high thermal conductivity and low linear expansion coefficient at low temperatures are favorable properties for stable operation of the cavity at high RF input power [3]. Motivated by these advantages, the development of a cryogenic C-band 2.6-cell photocathode electron gun has begun in 2013 at Nihon University in collaboration with KEK intending to use as the injector of a compact X-ray generating electron linac [4]. The cavity temperature of 20 K has been chosen by considering that the lowest surface resistance and the highest thermal conductivity are reached at around and below 20 K, and that a refrigerator with refrigeration capacity required for high power operation at 20 K is readily available.

From the result of the simulations for improvement of the power efficiency and the coupler property in the previous test cavity, a final cold model was fabricated in 2016 [5, 6]. The RF properties obtained at room temperature have been in good agreement with the CST Studio simulations [7]. The cryogenic experiments of the cavity carried out afterward have shown excellent results as expected.

This paper reports the characterization of the cold model cavity at 20 K measured by supplying the test RF power through a thermal insulating waveguide.

STRUCTURE OF THE 2.6-CELL CAVITY

The cryogenic C-band RF gun cavity consists of 5712 MHz $TM_{01\pi}$-mode 2.6 accelerating cells. The combination of a mode converter from rectangular TE_{10} to circular TM_{01} mode and a short circular waveguide, in a manner similar to an X-band RF gun [8], works as an input coupler that feeds the accelerating cells with the RF power along the cavity axis as shown in Fig. 1. The cavity dimensions were optimized to give high efficiency acceleration and low insertion loss in the converter by the simulations using Superfish and CST Studio [5, 6, 9].

The cavity, of high purity 6N8 copper, was fabricated at KEK with ultraprecision machining and diffusion bonding techniques. The diffusion bonding is considered to be an excellent method of fabrication to avoid the degradation of the surface resistance at low temperatures. Due to need for the measurement of the field on the cavity axis as a cold model, a hole with a diameter of 3.6 mm has been made in the center of the left-side end plate. Each cell is equipped with 4 tuners placed every 90º around the axis.
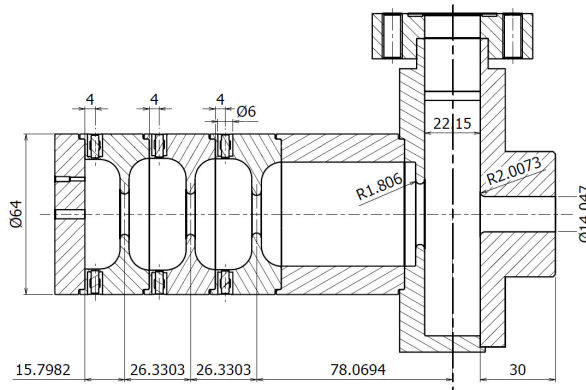

Figure 1: Cross-sectional view of the cold model of a C-band 2.6-cell RF gun cavity. The dimensions shown in the drawing are those for machining at 23.5 °C.

SHUNT IMPEDANCE AT ROOM TEMPERATURE

Figure 2 shows the behavior of the bead-pull perturbation measured on the cavity axis over the entire structure length, where the frequency shift is plotted at 0.5 mm step as an averaged result of 10 runs of the computer controlled automatic sweep. The radius r_b of the metal bead used in the measurement was 1.0 mm.

The frequency shift Δf of the $TM_{01\pi}$-mode resonant peak by the presence of the bead in the cavity is expressed as

$$\Delta f = -\frac{\pi \varepsilon_0 E_z^2 r_b^3}{U} f_0, \qquad (1)$$

where ε_0 is the dielectric constant of vacuum, f_0 the unperturbed frequency, E_z the axial electric field amplitude at the position of the bead and U the stored energy in the cavity [10]. The shunt impedance to quality factor ratio R/Q_0 is given by the relation

$$R/Q_0 = \left(\int |E_z| ds\right)^2 \Big/ 4\pi f_0 U, \qquad (2)$$

where $|E_z|$ is integrated along the axis over the 2.6 cells. Thus the ratio can be deduced from the frequency shift data by the perturbation method as

$$R/Q_0 = \left(\int \sqrt{|\Delta f|} ds\right)^2 \Big/ 4\pi^2 \varepsilon_0 f_0^2 r_b^3. \qquad (3)$$

The experimental ratio deduced from Eq. (3) has been R/Q_0 = 293 Ω in agreement with the result estimated by Eq. (2) from the axial field by the CST Studio simulation. In Fig. 2 the thin orange curve shows the frequency shift calculated by Eq. (1).

The effective maximum accelerating voltage V_{acc} in the 2.6-cell cavity without beam loading is given by

$$V_{acc} = \frac{2\sqrt{\beta}}{1+\beta} \sqrt{PZT^2 L}, \qquad (4)$$

where β is the input coupling coefficient of the cavity, P the source RF power, L the cavity length, Z ($= 2R/L$) the shunt impedance per unit length, and T ($= 0.763$) the transit time factor. Appling the unloaded quality factor $Q_0 = 13200$ at room temperature that has been reported elsewhere [5] and 16 % higher than the case in the previous cold model [11], the shunt impedance Z of the cavity is estimated to be 113 MΩ/m.
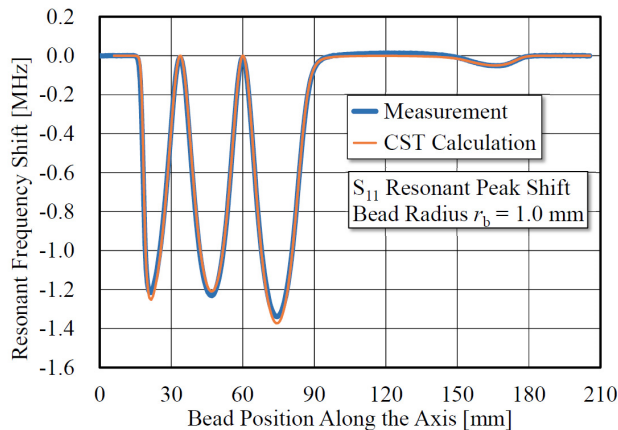

Figure 2: Result of the on-axis field measurement of the accelerating field by the bead-pull perturbation method.

CRYOGENIC SYSTEM ASSEMBLING FOR COLD TEST

Figure 3 shows the top view of the cryogenic system assembled for low-temperature cavity measurements. The cold model cavity is mounted on the cold head of the refrigerator (Suzuki Shokan RF273S) attached to the bottom

of the vacuum chamber. The chamber is pumped with a 250 l/sec turbo-molecular pump. The refrigeration capacity of the refrigerator is 5 W at 20 K. The test RF power from the network analyzer (Agilent E5071C) is supplied to the cavity through the R48-type waveguide inserted into the chamber.

The waveguide is made of stainless steel with 1.5 mm thick wall over a partial length of 275 mm [12]. The inner wall was plated with 20 μm thick copper. Figure 4 shows the picture of the cavity connected to the waveguide. The other end of the waveguide is connected to a coaxial-to-waveguide converter outside the chamber. The heat flow from the room-temperature end of the waveguide has been estimated to be 4 W. The network analyzer is calibrated at the waveguide flange of the converter before the vacuum chamber is pumped.
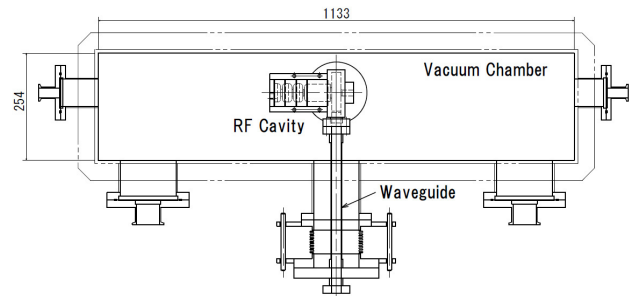

Figure 3: Top view of the cryostat assembled for the cold test of the cavity.
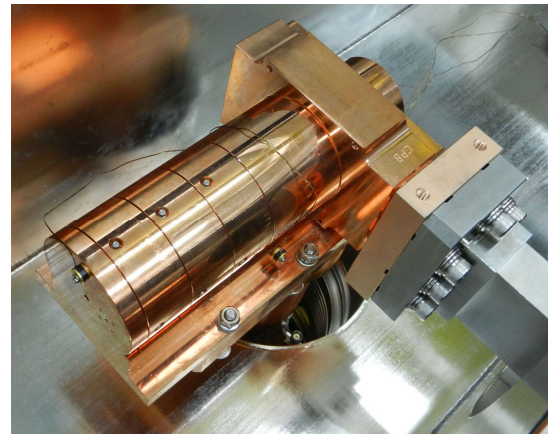

Figure 4: Picture of the cavity connected to the stainless steel waveguide.

EXPERIMENTS AND ANALYSES

The changes in the temperature and the resonant frequency of the cavity measured during a cooling experiment down to around 20 K are plotted in Fig. 5 as a function of the elapsed time since several minutes before the refrigerator was turned on. The cavity temperature was always monitored using 3 semiconductor thermometers attached to the different positions on the surface of the structure, i.e. (1) the 0.6-cell end plate, (2) near the cooling heatsink and (3) near the waveguide flange, respectively. In the course of the experiment the temperature was lowest at (2) and highest at (3) as expected. However, the difference was not

greater than 0.5 K, and less than 0.1 K at the temperatures below 35 K. The temperature data plotted in Fig. 5 is the result measured at the 0.6-cell end plate. The lowest cavity temperature reached by this cryogenic system was 19.61 K. No temperature stabilization has been done in the system.

The Smith Chart data and the temperatures of the cavity were taken every 2 minutes and stored in a PC simultaneously. The resonant frequency of the cavity at each temperature in Fig. 5 has been obtained by the least square fitting of the RF reflection coefficients in the vicinity of the resonance crest to a parabolic function. The frequency shift at the temperatures below 25 K has been less than 13 kHz. The average shift rate of 2.4 kHz/K over this region is approximately 1/40 of that in the room temperature region due to the small linear expansion coefficients of copper.
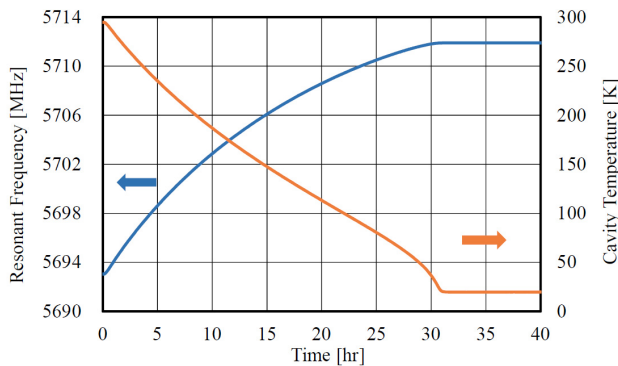

Figure 5: The temperature and the resonant frequency of the cold model cavity during a cooling experiment over 40 hours.

Examples of the RF reflection coefficients, $|S_{11}|$, around the resonant frequency measured at cavity temperatures of 294 K and 20 K are shown in Fig. 6. In both cases the vacuum chamber was pumped with a turbo-molecular pump. Each $|S_{11}|$ spectrum over ± 10 MHz around the peak frequency obtained in a series of experiments has been fitted to a Lorentzian curve by the least square fitting method to estimate the coupling coefficient and the loaded quality factor of the cavity.

The cooling experiments on this cold model were carried out 5 times in 3 months. The behavior of the Q_0 values evaluated from the analyses of the Smith Chart data is shown in Fig. 7 as a function of the cavity temperature for each measurement run. The different final Q_0 values resulted after cooled down to around 20 K can be related to
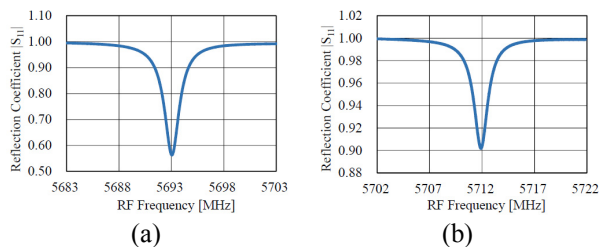

(a)   (b)

Figure 6: Examples of the RF reflection coefficients $|S_{11}|$ around the $TM_{01\pi}$ mode resonance measured at cavity temperatures of (a) 294 K and (b) 20 K.

the RF power loss in the coaxial cable which is very sensitive to ambient temperature.

The average values of the properties obtained from the experiments are listed in Table 1, where the values in parentheses are the results of the CST Studio simulations using the surface resistances based on the theory of the anomalous skin effect [2, 13]. Though the difference is not large, the resonant frequency shift caused by the cooling has been 0.12 MHz greater than that was estimated from the cavity contraction. The factor of increase in the frequency deduced from the NIST data [3] is denoted by an asterisk. The Q_0 values and the coupling coefficients are in agreement with the prediction by the CST Studio simulation.
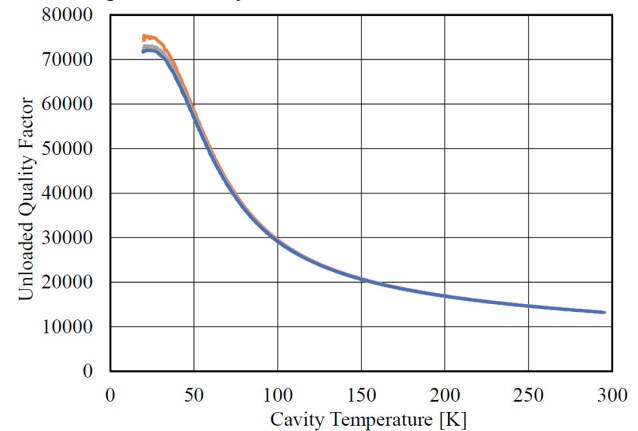

Figure 7: The behavior of the Q_0 values measured during 5 runs of the cooling experiment.

Table 1: The Properties Obtained by the Experiments

	at 296.65 K	at 20 K	ratio
Q_0	13176 ±20 (13310)	72775 ±1168 (73029)	5.52 ±0.09 (5.48)
coupling coefficient	3.566 ±0.008 (3.52)	19.79 ±0.26 (19.30)	5.55 ±0.07 (5.48)
resonant frequency [MHz]	5692.863±0.006 (5692.791)	5711.883±0.009 (5712.015)	1.0033409 *1.0033203

CONCLUSION

The cold model of a C-band 2.6-cell photocathode RF gun cavity has been characterized by the cryogenic cooling experiments. The unloaded quality factor of approximately 73000 at 20 K, with an enhancement factor of 5.2 from the room temperature operation, is in agreement with the result of the CST Studio calculation using the surface resistance based on the theory of the anomalous skin effect. The shunt impedance of 113 MΩ/m measured at room temperature corresponds to 624 MΩ/m at 20 K, which offers possibilities of high efficiency and high accelerating gradient RF guns at a high peak RF input power of the order of 10 MW: a peak field of 180 MV/m on the cathode surface is expected at 10 MW. Fabrication of a high power model cavity is under consideration for future high gradient experiments.

REFERENCES

[1] A. Septier, "The Surface Impedance of Superconducting Metals at High Frequencies", in *Linear Accelerators*, Ed. P. M. Lapostolle and A. L. Septier: North Holland Publishing (1970) pp. 1090-1092.

[2] G. E. H. Reuter and E. H. Sondheimer, "The theory of the anomalous skin effect in metals", Proc. the Royal Soc. of London A, Mathematical and Physical Sciences, 195 (1948), pp. 336-364.

[3] http://cryogenics.nist.gov/MPropsMAY/OFHC%20Copper/OFHC_Copper_rev.htm

[4] M. Fukuda *et al.*, "Status and Future Plan of the Development of a Compact X-ray Source Based on ICS at Laser Undulator Compact Xray (LUCX)", In *Proc. NA-PAC13*, Pasadena, CA, USA, September 2013, paper TUPMA01, pp. 589-591 (2013).

[5] T. Sakai *et al.*, "Cold Model Cavity for 20-K Cryocooled C-band Photocathode RF Gun", In *Proc. IPAC'16*, Busan, Korea, May 2016, paper WEPMY037, pp. 2635-2637.

[6] K. Takatsuka *et al.*, "Optimization of C-band RF Input Coupler as a Mode Converter for 20-K Cryocooled Photocathode RF Gun", In *Proc. IPAC'16*, Busan, Korea, May 2016, paper WEPMY038, pp. 2638-2640.

[7] CST Studio Suite^TM, CST AG, Germany, http://www.cst.com

[8] Y. Taniguchi *et al.*, "Development of X-band thermionic RF electron gun using choke structure", in *Proc. 5th Annual Meeting of Particle Accelerator Society of Japan*, August 2008, Higashihiroshima, Japan, pp. 954-956 (in Japanese).

[9] J. H. Billen and L. M. Young, LA-UR-96-1834 (2006), Los Alamos National Laboratory, http://laacg.lanl.gov/laacg/services/download_sf.phtml

[10] E. L. Ginzton, *Microwave Measurements*. McGraw-Hill (1957).

[11] T. Tanaka *et al.*, "RF Input Coupler for 20 K Cooled C-band 2.6-cell Photocathode RF Gun", in *Proc. IPAC'15*, Richmond, VA, USA, May 2015, paper WEPWA015, pp.2522-2525.

[12] A. Iino *et al.*, "High-Power Test of the C-band Accelerating Structure with a High-Q factor at 20 K", in *Proc. 13th Annual Meeting of Particle Accelerator Society of Japan*, August 2016, Chiba, Japan, pp.863-866 (in Japanese).

[13] T. Tanaka *et al.*, "Basic Design of a 20K C-band 2.6-cell Photocathode RF Gun", in *Proc. IPAC'14*, Dresden, Germany, June 2014, paper MOPRI030, pp. 658-660.

03 Novel Particle Sources and Acceleration Techniques

T02 Electron Sources